

Microwave-mediated synthesis of spinel CuAl_2O_4 nanocomposites for enhanced electrochemical and catalytic performance

Ratiram Gomaji Chaudhary¹  · Vaishali N. Sonkusare² · Ganesh S. Bhusari³ · Aniruddha Mondal⁴ · Dadamia PMD Shaik⁵ · Harjeet D. Juneja²

Received: 8 September 2017 / Accepted: 17 November 2017
© Springer Science+Business Media B.V., part of Springer Nature 2017

Abstract The present study explores synthesis of spinel copper aluminate nanocomposites (CuAl_2O_4 NCs) for electrochemical applications and solvent-free synthesis of xanthenedione derivatives. CuAl_2O_4 NCs were synthesized from copper nitrate and aluminum nitrate with/without use of sodium dodecyl sulfate (SDS) by aqueous precipitation and microwave-assisted (MW) technique. As-synthesized CuAl_2O_4 NCs were characterized structurally and morphologically using X-ray diffraction (XRD) analysis, Fourier-transform infrared (FT-IR) spectroscopy, diffuse reflectance spectroscopy (DRS), energy-dispersive X-ray spectroscopy (EDS), X-ray photoelectron spectroscopy (XPS), Raman spectroscopy, scanning electron microscopy (SEM), transmission electron microscopy (TEM), and atomic force microscopy (AFM). Formation of cubic spinel structure after calcination at 900 °C was confirmed by XRD analysis, while Raman, XPS, and EDS validated the composition and purity. TEM revealed that the particles had uniform nanosphere shape with average size of 10 nm for microwave-assisted with surfactant (MWS- CuAl_2O_4), while aqueous precipitation with surfactant (APS- CuAl_2O_4) NCs exhibited nanograins with particle size of 17 nm. AFM revealed higher surface roughness

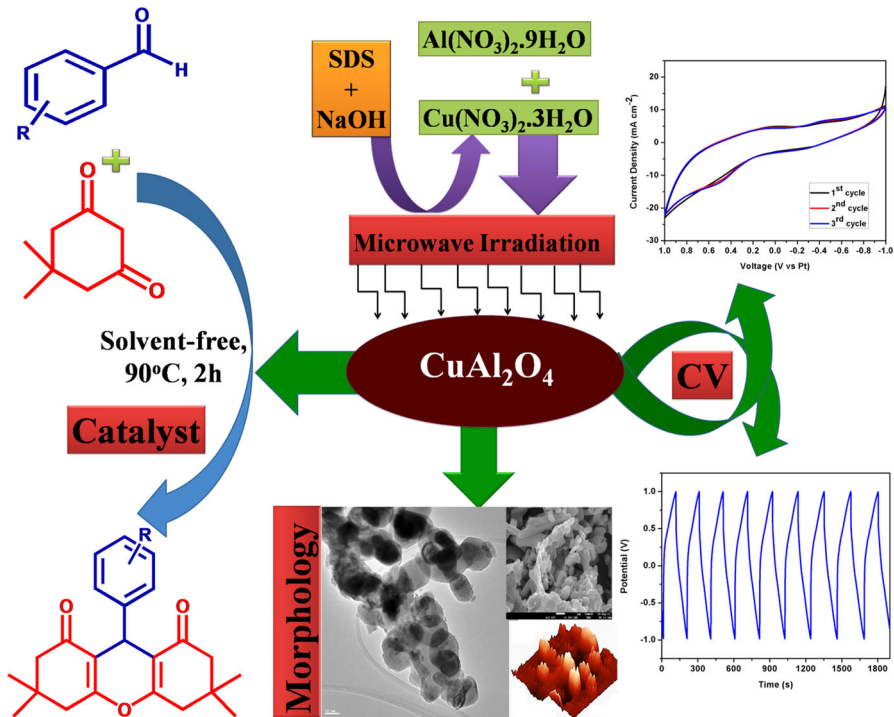
Electronic supplementary material The online version of this article (<https://doi.org/10.1007/s11164-017-3213-z>) contains supplementary material, which is available to authorized users.

✉ Ratiram Gomaji Chaudhary
chaudhary_rati@yahoo.com

- ¹ Post Graduate Department of Chemistry, Seth Kesarimal Porwal College of Arts, Commerce and Science, Kamptee 441001, India
- ² Post Graduate Teaching Department Chemistry, Rashtrasant Tukadoji Maharaj Nagpur University, Nagpur 440033, India
- ³ Department of Chemistry, Visvesvaraya National Institute Technology (VNIT), Nagpur 440010, India
- ⁴ Discipline of Inorganic Materials and Catalysis, Academy of Scientific and Innovative Research, CSIR-Central Salt and Marine Chemical Research Institute, Bhavnagar 364002, India
- ⁵ Department of Physics, Sree Vidhyaniketan Engineering College, Tirupati 517102, India

for MWS-CuAl₂O₄ NCs than APS-CuAl₂O₄ NCs. The electrochemical performance of the CuAl₂O₄ NCs was examined in aqueous Na₂SO₄ (1 M) as electrolyte using cyclic voltammetry (CV), revealing that the MWS-CuAl₂O₄ NCs demonstrated high specific capacitance (125 F g⁻¹ at current density of 0.5 mA cm⁻²). Furthermore, one-pot, facile, eco-friendly MWS-CuAl₂O₄ NC-catalyzed synthesis of xanthenediones was developed, exhibiting excellent yield and reusability with negligible reduction in efficiency even after four consecutive cycles.

Graphical Abstract MWS-CuAl₂O₄ NCs showed enhanced electrochemical and catalytic performance.



Keywords Spinel CuAl₂O₄ NCs · Microwave-assisted technique · Electron microscopy · Nanospheres · Electrochemical performance · Heterogeneous catalyst

Introduction

Nowadays, heterogeneous catalysts are attracting much attention from the scientific community due to their diverse properties and applications [1–8]. Among such materials, spinel copper aluminate nanocomposites (CuAl₂O₄ NCs) are materials of interest due to their non-toxic nature, low-cost, high thermal stability, high

mechanical strength, hydrophobicity, and low surface acidity [9], characteristics that make them widely applicable in various fields, e.g., as photocatalysts for degradation of organic pollutants, as magnetic materials, in rechargeable batteries, for organic transformations, in medicine, and for recycling of nuclear fuel [10–12].

Various methods, including solid-state, co-precipitation, hydrothermal, sonochemical, reverse microemulsion, sol–gel reaction, and microwave technique, have been employed for preparation of CuAl_2O_4 NCs [13–18]. Among these methods, the microwave approach is a valuable and attractive technique for preparation of CuAl_2O_4 NCs, due to its high reaction rate, short reaction time, high yield, and selectivity [18]. Also, it produces pure and ultrafine powder at relatively low temperature because of its different heating mechanism compared with conventional techniques, opening up prospects for manufacture of diverse materials in very short time with high energy efficiency [19]. Numerous researchers have prepared different aluminate nanocomposites, including CoAl_2O_4 , $\text{Co:ZnAl}_2\text{O}_4$, ZnAl_2O_4 , MgAl_2O_4 , $\text{ZnAl}_2\text{O}_4/\text{ZnO}$, $\text{Ni-MgX-Al}_2\text{O}_3$, SrAl_2O_4 , etc., using microwave-assisted technique [20–25].

Synthesis of xanthenediones is an ongoing hot topic of research, due to their use as pharmacophores and valuable reactive intermediates in both synthetic and medicinal chemistry [26]. However, development of eco-friendly methods for synthesis of xanthenedione derivatives remains a challenge. Various researchers have reported CuAl_2O_4 NCs for photocatalytic degradation of methyl orange [9, 27]. Kwak et al. synthesized CuAl_2O_4 NCs via a sol–gel method for hydrogenolysis of glycerol [13]. However, there is only a single report on microwave combustion preparation of spinel CuAl_2O_4 NCs for catalytic oxidation of benzyl alcohol [18]. To the best of the authors' knowledge, the electrochemical properties of CuAl_2O_4 NCs also remain unexplored. Furthermore, no reports are available on solvent-free green synthesis of xanthenediones using microwave-irradiated CuAl_2O_4 NCs as catalyst.

The authors previously reported preparation of new, efficient, reusable copper and alumina as nanocatalysts for fabrication of chromene derivatives and dihydropyrimidinones, respectively [28, 29]. In the work presented herein, spinel CuAl_2O_4 NCs were synthesized by adopting aqueous precipitation (AP) and microwave-assisted (MW) techniques with/without use of SDS as surfactant. As-synthesized NCs were characterized by various techniques including XRD analysis, FT-IR spectroscopy, DRS, EDS, XPS, Raman spectroscopy, SEM, TEM, and AFM. Furthermore, the electrochemical performance of the synthesized NCs was investigated. The prepared MWS- CuAl_2O_4 NCs were then used as nanocatalyst for synthesis of xanthenediones, and reaction conditions including time, temperature, and solvents were optimized, and their reusability investigated.

Experimental

Materials and methods

Copper nitrate trihydrate [$\text{Cu}(\text{NO}_3)_2 \cdot 3\text{H}_2\text{O}$], aluminum nitrate nonahydrate [$\text{Al}(\text{NO}_3)_3 \cdot 9\text{H}_2\text{O}$], sodium hydroxide (NaOH), sodium dodecyl sulfate (SDS), and sodium sulfate (Na_2SO_4) were procured from Sigma-Aldrich (Germany). Polyvinylidene fluoride (PVDF), acetone, ethanol, ethyl acetate, chloroform, *N*-methyl-2-pyrrolidone (NMP), and dichloroethane were purchased from Merck (India). All chemical reagents were of analytical grade and used without further purification.

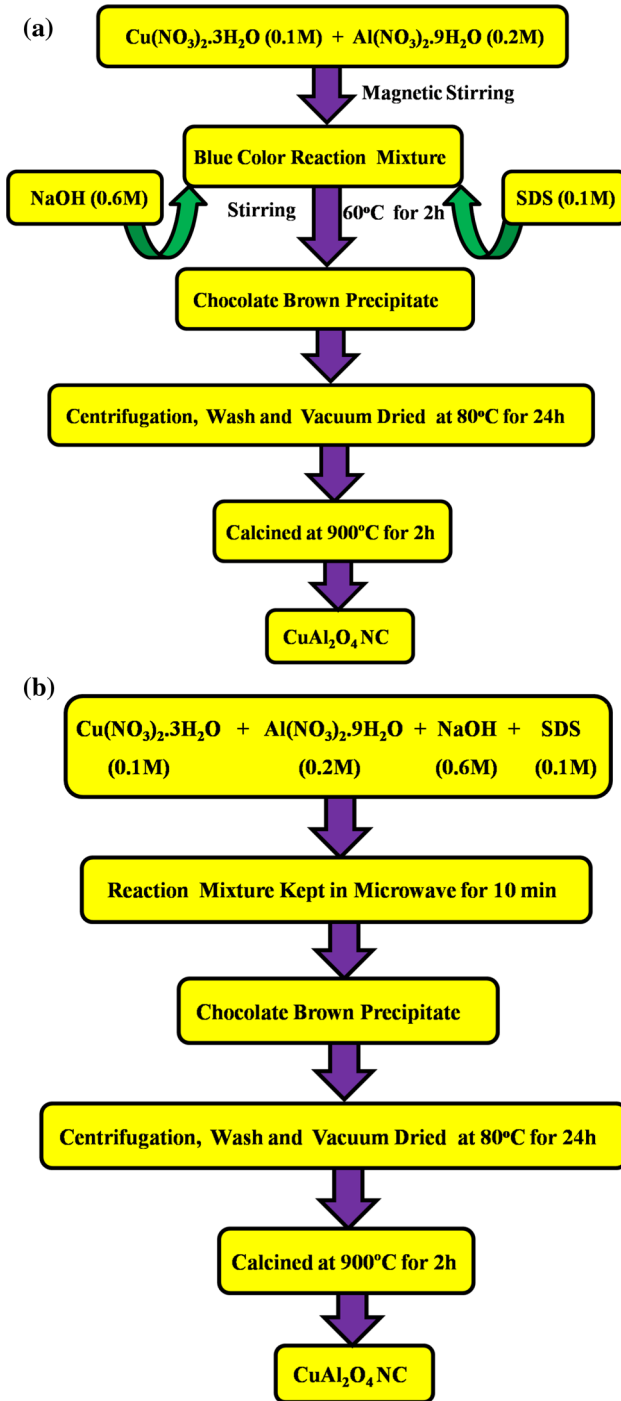
Synthesis of CuAl_2O_4 NCs

CuAl_2O_4 NCs were synthesized from $\text{Cu}(\text{NO}_3)_2 \cdot 3\text{H}_2\text{O}$ and $\text{Al}(\text{NO}_3)_3 \cdot 9\text{H}_2\text{O}$ at molar ratio of $\text{Cu}/\text{Al} = 1:2$ with/without use of SDS as surfactant by AP and MW-assisted methods. Aqueous solution of $\text{Cu}(\text{NO}_3)_2 \cdot 3\text{H}_2\text{O}$ (0.1 M) and $\text{Al}(\text{NO}_3)_3 \cdot 9\text{H}_2\text{O}$ (0.2 M) was prepared by dissolving separately in deionized water. Then, both solutions were transferred into a round-bottomed flask (RBF), and stirred well by magnetic stirrer until clear blue solution formed. Afterward, freshly prepared NaOH (0.6 M) and SDS (0.1 N) solution was added, and the reaction mixture was maintained at 60 °C for 2 h. Then, chocolate-brown precipitate was obtained, which was separated by centrifugation and further washed with distilled water, ethanol, and acetone. NCs synthesized by aqueous precipitation technique with and without SDS are denoted as APS- CuAl_2O_4 and AP- CuAl_2O_4 , respectively.

In addition, $\text{Cu}(\text{NO}_3)_2 \cdot 3\text{H}_2\text{O}$ (0.1 M) and $\text{Al}(\text{NO}_3)_3 \cdot 9\text{H}_2\text{O}$ (0.2 M), NaOH (0.6 M), and SDS (0.1 M) were taken in a RBF. Then, the mixture was placed in a microwave (Sinerio, 1 kW) for 10 min for irradiation. Chocolate-brown precipitate was obtained, which was separated using the above-mentioned filtration and washing procedures. NCs prepared with and without use of SDS by MW-assisted technique are denoted as MWS- CuAl_2O_4 and MW- CuAl_2O_4 , respectively. After washing, as-synthesized NC precipitates were dried in a vacuum oven at 80 °C for 24 h. Then, vacuum oven-dried CuAl_2O_4 NCs (AP- CuAl_2O_4), APS- CuAl_2O_4 , MW- CuAl_2O_4 , and MWS- CuAl_2O_4) were calcined at 900 °C for 2 h to achieve nanosized dimension. A flowchart of the synthesis of CuAl_2O_4 NCs through AP and MW-assisted techniques is presented in Scheme 1.

Characterization techniques

X-ray diffraction (XRD) measurement was performed on a Bruker AXS D8 Advance diffractometer in the 2θ range from 20° to 80° using Cu K_α radiation at $\lambda = 0.154$ nm. Fourier-transform infrared (FT-IR) spectra were recorded in the range from 400 to 4000 cm^{-1} on a Bruker IFS 66v spectrophotometer having 4.0 cm^{-1} resolution by KBr pellet technique. Qualitative elemental analysis was performed using energy-dispersive X-ray spectroscopy (EDS; Oxford Instrument).



Scheme 1 Synthesis of CuAl_2O_4 NCs through a AP and b MW-assisted techniques

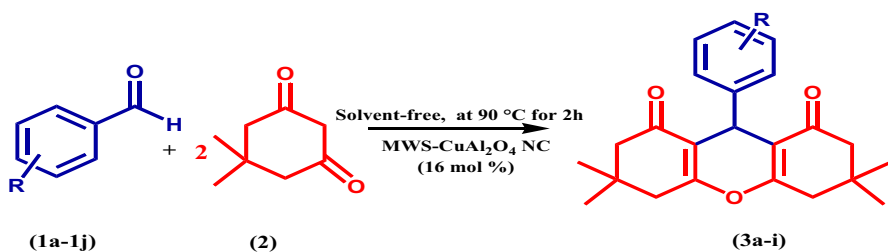
Ultraviolet–visible (UV–Vis) diffuse reflectance spectra were recorded on a Cary 100UV spectrophotometer. Raman spectra were obtained using a JY Horiba HR-800 spectrophotometer. X-ray photoelectron spectroscopy (XPS, Sigma Probe, Thermo-VG) was performed using a monochromatic Al K_{α} X-ray source for exciting photoelectrons. Scanning electron microscopy (SEM, JEOL JSM-690LV) and transmission electron microscopy (TEM, JEOL-JEM 100SX) were used to study the surface morphology, while surface roughness was analyzed by atomic force microscopy (AFM; DNN).

Electrochemical performance

The working electrode was prepared from homogeneous mixture of CuAl_2O_4 NC powder (80%), carbon black (10%), and PVDF (10%) as binder. The above mixture was ground for 30 min, then homogeneous slurry was made using NMP as solvent. The slurry was subsequently brush-coated onto chemically cleaned pure stainless-steel plate. To evaporate the solvent, the electrode was kept in an air drying oven at 100 °C for 2 h. The electrochemical properties of the CuAl_2O_3 NCs were examined using an electrochemical analyzer (CHI608C) equipped with three-electrode glass cells, with CuAl_2O_4 as working electrode, platinum foil as counter and reference electrode, and 1 M Na_2SO_4 as electrolyte.

Solvent-free synthesis of xanthenedione derivatives

Aromatic aldehyde and dimedone were taken in a RBF at 1:2 mmol ratio along with synthesized MWS- CuAl_2O_4 NCs (16 mol%) as catalyst, and the reaction mixture was stirred and refluxed at 90 °C for 2 h. MWS- CuAl_2O_4 -catalyzed synthesis of xanthenediones is portrayed in Scheme 2. Reaction progress was monitored by thin-layer chromatography (TLC) using ethyl acetate/petroleum ether (3:7) as solvents. At reaction completion, the reaction mixture was cooled to room temperature (25 ± 2 °C), then the product was dissolved with methylene dichloride (15 ml) and the NCs separated by filtration for the next trial without any further treatment. The reaction mixture was concentrated on a rotary evaporator at reduced pressure. The residue was purified and recrystallized. The physical parameters of the derivatives are presented in Table 1.



Scheme 2 Synthesis of xanthenediones using prepared MWS- CuAl_2O_4 NCs as nanocatalyst

Table 1 MWS-CuAl₂O₄-catalyzed synthesis of xanthenedione derivatives (**3a–i**)

Entry	Product	Ar	Time (h)	Yield (%)	Color	M.p. (°C)
1	3a	C ₆ H ₅	3	87	Green	202–204
2	3b	4-ClC ₆ H ₄	4	80	Brown	228–230
3	3c	3-ClC ₆ H ₄	3	78	Green	180–182
4	3d	2-ClC ₆ H ₄	4.5	82	Green	226–228
5	3e	4-BrC ₆ H ₄	3	86	Green	238–239
6	3f	3-BrC ₆ H ₄	6	72	Green	188–190
7	3g	2-BrC ₆ H ₄	3	82	Green	226–229
8	3h	4-NO ₂ C ₆ H ₄	3	77	Green	225–227
9	3i	3-NO ₂ C ₆ H ₄	4	74	Green	167–169

Table 2 Xanthenedione derivatives synthesized with and without solvents

Entry	Solvent	Time (h)	Yield (%) ^a
1	H ₂ O	3	–
2	C ₂ H ₅ –OH	3	20 ± 01
3	CH ₃ –COOC ₂ H ₅	3	58 ± 01
4	CHCl ₃	3	–
5	CH ₂ Cl ₂	3	–
6 ^a	Solvent free	2	87 ± 01

^aIsolated yield

Selected spectral data for typical compounds are given below:

1. N-Benzylidene-1H-benzo[d]imidazol-2-amine (Table 2; 3a) Green solid; FT-IR (KBr): 3686, 2609, 2916, 2221, 1592, 1524, 1208, 1150, 950 cm⁻¹; ¹H-NMR (400 MHz, DMSO-*d*₆) δ, ppm: 11.87 (s, 1H, NH), 7.28–7.08 (m, 9H, H *Arom.*), and 5.54 (s, 1H, CH).

2. N-(4-Nitrobenzylidene)-1H-benzo[d]imidazol-2-amine (Table 1; 3b) Brown solid; FT-IR (KBr): 3167, 3080, 1614, 1591, 1514, 1425, 1342, 1228, 1109, 833, 763, 680, 441 cm⁻¹; ¹H-NMR (400 MHz, DMSO-*d*₆) δ, ppm: 11.89 (s, 1H, NH), 9.58 (s, 1H, CH), 7.37–7.16 (m, 4H, H *Arom.*), and 6.60–6.20 (m, 4H, H *Arom.*).

3. N-(2-Chlorobenzylidene)-1H-benzo[d]imidazol-2-amine (Table 1; 3g) Green solid; FT-IR (KBr): 3053, 2986, 1604, 1520, 1427, 1273, 1053, 756, 684, 451 cm⁻¹; ¹H-NMR (400 MHz, DMSO-*d*₆) δ, ppm: 12.86 (s, 1H, NH), 9.78 (s, 1H, CH), 8.28 (d, *J* = 7.7 Hz, 1H, H *Arom.*), 7.65–7.48 (m, 5H, H *Arom.*), and 7.21 (q, 2H, H *Arom.*).

4. N-(4-Chlorobenzylidene)-1H-benzo[d]imidazol-2-amine (Table 1; 3d) Green solid; FT-IR (KBr): 3375, 3065, 2993, 1612, 1570, 1500, 1429, 1311, 1234, 1089, 821, 738, 505 cm⁻¹; ¹H-NMR (400 MHz, DMSO-*d*₆) δ, ppm: 12.86 (s, 1H, NH), 9.46 (s, 1H, CH), and 8.08–7.18 (m, 8H, H *Arom.*).

5. *N*-(4-Bromobenzylidene)-1*H*-benzo[*d*]imidazol-2-amine (Table 1; 3f) Green solid; FT-IR (KBr): 3422, 3063, 2991, 1610, 1489, 1429, 1070, 819, 738 cm^{-1} ; $^1\text{H-NMR}$ (400 MHz, $\text{DMSO-}d_6$) δ , ppm: 12.75 (s, 1H, NH), 9.44 (s, 1H, CH), and 7.99–7.18 (m, 8H, H *Arom.*).

6. *N*-(3-Nitrobenzylidene)-1*H*-benzo[*d*]imidazol-2-amine (Table 1; 3c) Green solid; FT-IR (KBr): 3346, 3088, 1608, 1529, 1431, 1350, 1278, 1085, 742, 665 cm^{-1} ; $^1\text{H-NMR}$ (400 MHz, $\text{DMSO-}d_6$) δ , ppm: 12.86 (s, 1H, NH), 9.61 (s, 1H, CH), and 8.88–7.21 (m, 8H, H *Arom.*).

Results and discussion

XRD patterns of CuAl_2O_4 NCs using the different synthetic techniques are shown in Fig. 1. All the CuAl_2O_4 NCs showed diffraction peaks at $2\theta = 35.53^\circ$, 38.68° , 48.82° , 53.44° , 58.43° , and 66.82° , corresponding to (*hkl*) values of (220), (311), (400), (411), (511), and (440), respectively. The diffraction peaks are in agreement with Joint Committee on Powder Diffraction Standards (JCPDS) standard card no. 76-2295, indicating cubic spinel structure for CuAl_2O_4 . Average crystallite size of 3.5 and 2.0 nm was estimated for APS- CuAl_2O_4 and MWS- CuAl_2O_4 NCs, respectively, using the Scherrer equation. Wide diffraction peaks (Fig. 1a & b) were observed for AP- CuAl_2O_4 NCs, while comparatively sharp peaks were seen for APS- CuAl_2O_4 NCs. Moreover, sharper diffraction peaks were observed for MW-assisted (MW- CuAl_2O_4 and MWS- CuAl_2O_4) NCs (Fig. 1c & d). An absence of diffraction peaks corresponding to CuO and Al_2O_3 in the XRD patterns, indicates formation of cubic spinel CuAl_2O_4 structure at 900°C through diffusion of CuO into the Al_2O_3 lattice [30]. The EDS spectra of the as-synthesized CuAl_2O_4 NCs are

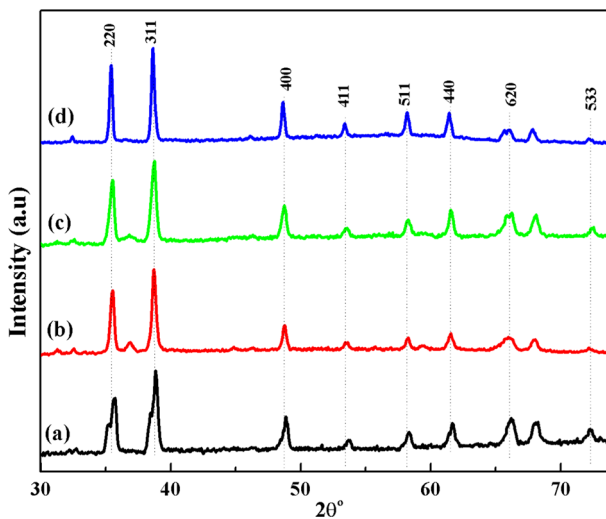


Fig. 1 XRD patterns of (a) AP- CuAl_2O_4 , (b) APS- CuAl_2O_4 , (c) MW- CuAl_2O_4 , and (d) MWS- CuAl_2O_4

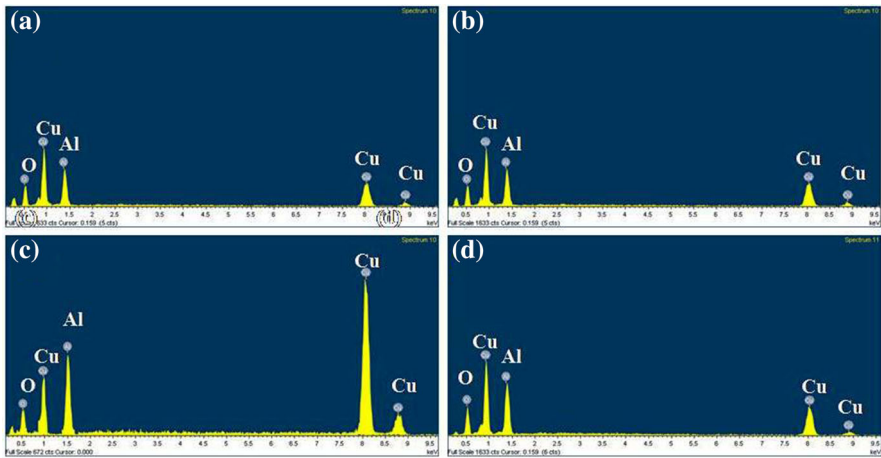


Fig. 2 EDS spectra of **a** AP- CuAl_2O_4 , **b** APS- CuAl_2O_4 , **c** MW- CuAl_2O_4 , and **d** MWS- CuAl_2O_4

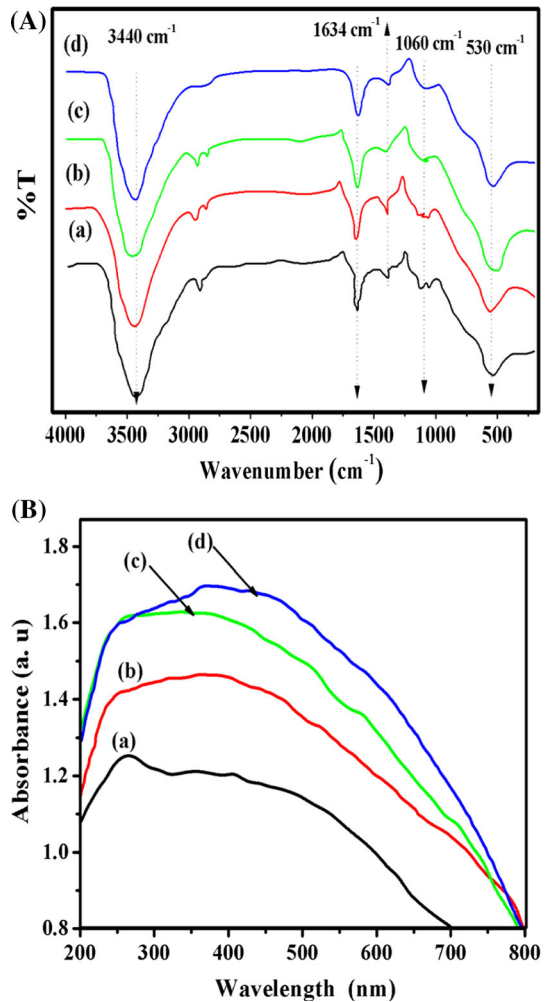
shown in Fig. 2, providing evidence of presence of Cu, Al, and O elements as well as pure CuAl_2O_4 phase. Moreover, no traces of other elements were found, thus confirming the purity of the CuAl_2O_4 NCs, in good agreement with the XRD results. Moreover, elemental analysis revealed composition of 13.01% Cu, 28.59% Al, and 58.39% O (atomic percent) according to the spectra of the CuAl_2O_4 NCs, close to the theoretical composition (14.29% Cu, 28.57% Al, and 57.17% O). These results therefore confirm the Cu-to-Al atomic stoichiometry of 1:2 in the CuAl_2O_4 NCs.

Further, the confirmation of CuAl_2O_4 structure was provided by the FT-IR (Fig. 3A). Absorbance bands observed at 617, 709, and 810 cm^{-1} were assigned to Cu–O, Al–O, and Cu–O–Al bonds, respectively, while peaks located at around 1689 and 3500 cm^{-1} were ascribed to H–O–H bending and O–H stretching vibration, attributed to presence of moisture. The observation of signals corresponding to Cu–O, Al–O, and Cu–O–Al bonds again confirms the structure [31] of the CuAl_2O_4 NCs, in good agreement with the XRD and EDS results.

The UV-DRS spectra of CuAl_2O_4 NCs are shown in Fig. 3B. The CuAl_2O_4 NCs exhibited a similar absorption band at around 390 nm (Fig. 3B), indicating formation of NC particles with similar phase. However, the initial peak of the AP- CuAl_2O_4 NCs showed prominent lower absorbance at 265 nm due to metal–metal charge transition only, after which the absorbance increased at around 390–450 nm, indicating nucleation, growth, and reduction of particle size because of surfactant doping of NCs.

Furthermore, the NC samples were examined by Raman spectroscopy, which is extensively used for determining the structure of materials, being especially useful for spinels. The Raman signals of aluminates enable examination of the internal vibrations of Al_2O_4 tetrahedra [32, 33]. The Raman shifts of the spinel CuAl_2O_4 NCs were collected in the spectral range from 255 to 650 cm^{-1} (Fig. 4). The vibrational peaks observed at 299.98 and 255.56 cm^{-1} for AP- CuAl_2O_4 NCs, APS- CuAl_2O_4 NCs, MW- CuAl_2O_4 NCs, and MWS- CuAl_2O_4 NCs were ascribed to asymmetric and symmetric bending vibration of Al_2O_4 . Other vibrational peaks at

Fig. 3 **A** FT-IR spectra and **B** UV-DRS of (a) AP-CuAl₂O₄, (b) APS-CuAl₂O₄, (c) MW-CuAl₂O₄, and (d) MWS-CuAl₂O₄



388.55 and 342.22 cm⁻¹ observed for AP-CuAl₂O₄ NCs and MWS-CuAl₂O₄ NCs were assigned to external vibrational modes. Vibrational peaks observed at 632.21, 620.26, 615.42, and 621.52 cm⁻¹ for AP-CuAl₂O₄ NCs, APS-CuAl₂O₄ NCs, MW-CuAl₂O₄ NCs, and MWS-CuAl₂O₄ NCs correspond to asymmetric and symmetric Al–O stretching modes, respectively. This peak was attributed F_{2g} character and assigned to Al–O stretching modes of the Al₂O₄ group. The values of these peaks are in accordance with those reported in literature [34, 35]. The Raman spectra also show a shoulder peak of the E_g mode for the synthesized NCs, which may correspond to the bending mode of Al ions. Interestingly, the spectra clearly show formation of CuAl₂O₄ NCs. Overall, these results reveal that the type of aluminate spinel investigated in the present work is a normal spinel with CuAl₂O₄ structure.

Furthermore, the chemical state of elements in the CuAl₂O₄ NCs were investigated by XPS and the results are shown in Fig. 5(a–d). The XPS spectrum

Fig. 4 Raman spectra of (a) AP- CuAl_2O_4 , (b) APS- CuAl_2O_4 , (c) MW- CuAl_2O_4 , and (d) MWS- CuAl_2O_4 NCs

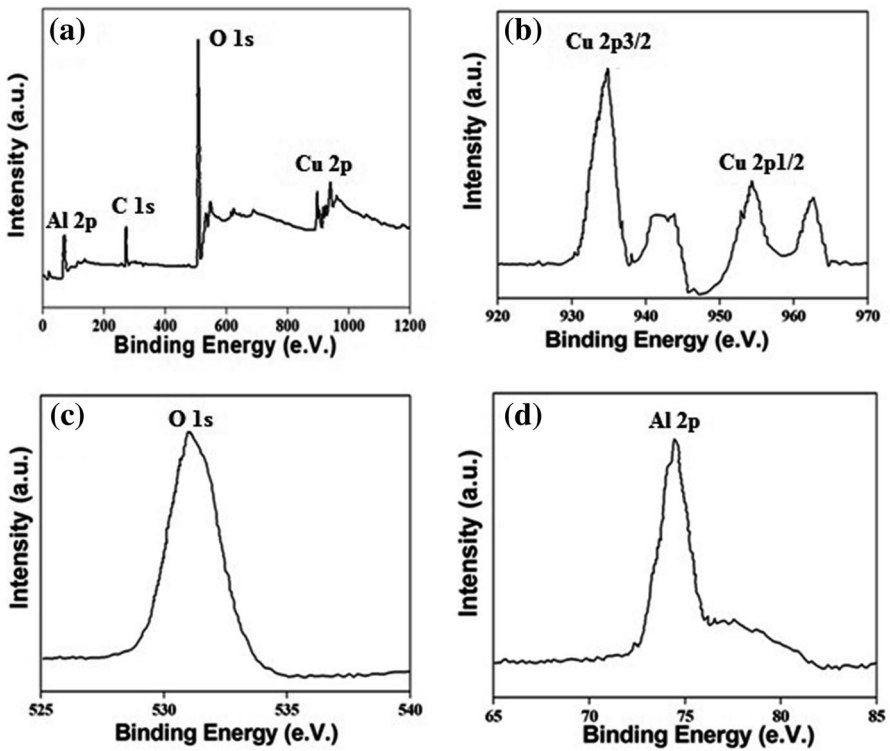
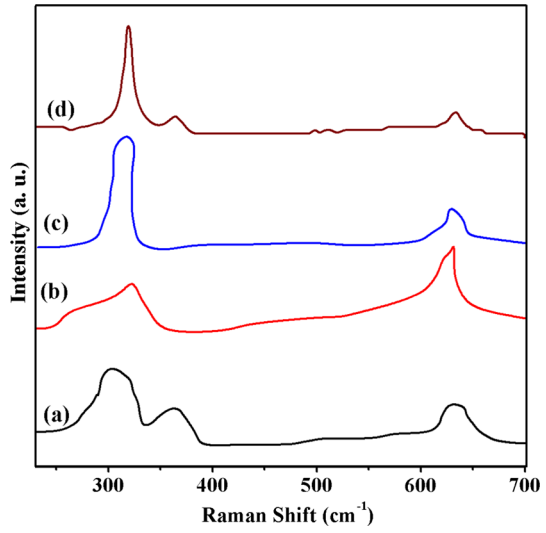


Fig. 5 XPS spectra of MWS- CuAl_2O_4 NCs

(Fig. 5a) of MWS-CuAl₂O₄ NCs revealed presence of aluminum (Al), oxygen (O), copper (Cu), and carbon (C) peaks. Cu 2*p* peaks were observed at 932 and 952 eV, assigned to Cu 2*p*_{3/2} and Cu 2*p*_{1/2} (Fig. 5b), respectively, in agreement with literature [36]. The XPS results confirmed the electronic state of Cu in the CuAl₂O₄ NCs to be + 2. Peaks for O were observed at around 531 eV, confirming presence of O²⁻ (Fig. 5c), while the peaks at 74.5 eV for Al correspond to the Al³⁺ state (Fig. 5d). Furthermore, a small satellite peak of C was observed at 280 eV, which comes from the XPS instrument itself due to unintentional presence of hydrocarbon.

Subsequently, the surface morphology, size, interfaces, crystallinity, and surface roughness of the as-synthesized NCs were examined by SEM, TEM, and AFM. SEM images of AP-CuAl₂O₄ NCs showed microflake-like morphology with agglomeration (Fig. 6a–c), while APS-CuAl₂O₄ NCs showed uniform fine microflake morphology (Fig. 6d–f) with reduced size and no aggregation, plus cashew nut-like shape (Fig. 6f). However, the surface morphology of CuAl₂O₄ NCs changed when synthesized with MW assistance. MW-CuAl₂O₄ NCs showed mixed-type morphologies including microrod, microsphere, rectangular plate, and microtube (Fig. 6g–i), whereas MWS-CuAl₂O₄ NCs exhibited layers of microrods with extended homogeneity (Fig. 6j–l). Hence, the formation of the mixed morphology when using both techniques confirms the formation of the composites. Next, the surface morphology, particle size, and interfaces of the synthesized CuAl₂O₄ NCs were examined by TEM (Fig. 7). TEM images of AP-CuAl₂O₄ NCs revealed agglomerated nanoflake morphology of copper oxide covered by porous aluminate material with fine interface formation (Fig. 7a–b) having particle size of 20 nm. However, APS-CuAl₂O₄ NCs showed nanograin-like structure (Fig. 7c–d) with particle size of 17 nm and reduced aggregation compared with the AP-CuAl₂O₄ NCs. The reduction in particle size indicates formation of interfaces between two particles. According to this principle, fast and uncontrolled coagulation occurred during precipitation and the inherent tendency of nanostructures to reduce their surface energy can explain the observed agglomeration of the CuAl₂O₄ NCs [37]. The MW-CuAl₂O₄ NCs (Fig. 7e–h) showed little agglomeration compared with the NCs synthesized through AP (AP-CuAl₂O₄ and APS-CuAl₂O₄), while the MWS-CuAl₂O₄ NCs exhibited uniform nanosphere shape (Fig. 7g–h) with particle size of 10 nm. Figure 7(e–f) clearly shows the surface of copper oxide nanoparticles coated with aluminate porous materials with fine interface formation. Such production of uniform, minimally agglomerated spheres occurs because of homogeneous nucleation during rapid MW heating. In contrast, in the conventional (AP) heating mode, the time for nucleation may be sufficient, but the presence of various heating zones will lead to formation of larger particles with a wider distribution [37]. It was observed that formation of NCs by either the usual heating or microwave-assisted method depended on the heating mechanism. These results imply that the synthesis protocol applied (AP or MW) has a dominant influence on the surface morphology and average particle size of the CuAl₂O₄ NCs owing to their different heating mechanisms [38, 39]. Finally, TEM revealed that copper oxide NPs were interfaced with aluminate surface (Figs. 6 & 7), with two crystal structures on the composite surfaces, again corroborating successful synthesis of NCs.

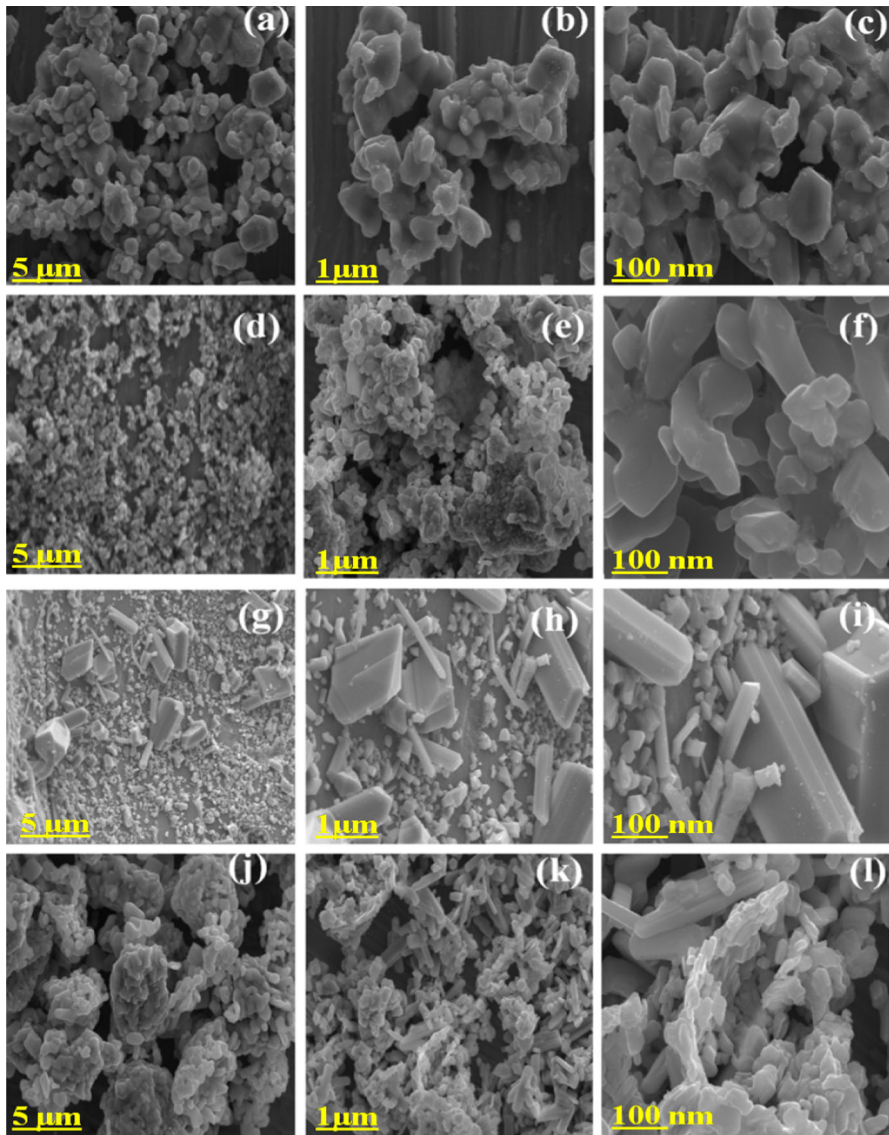


Fig. 6 SEM images of **a–c** AP- CuAl_2O_4 , **d–f** APS- CuAl_2O_4 , **g–i** MW- CuAl_2O_4 , and **j–l** MWS- CuAl_2O_4 NCs

Furthermore, the surface roughness of the NCs was examined by AFM (Fig. 8a & b). AFM images revealed almost constant, uniform height profile (of around 7 nm) for the APS- CuAl_2O_4 NCs (Fig. 8a), and a slightly higher height profile (of around 10 nm) for the MWS- CuAl_2O_4 NCs (Fig. 8b). However, uneven surface roughness was seen for the APS- CuAl_2O_4 NCs and MWS- CuAl_2O_4 NCs. Comparatively higher surface roughness was shown by the MWS- CuAl_2O_4 NCs

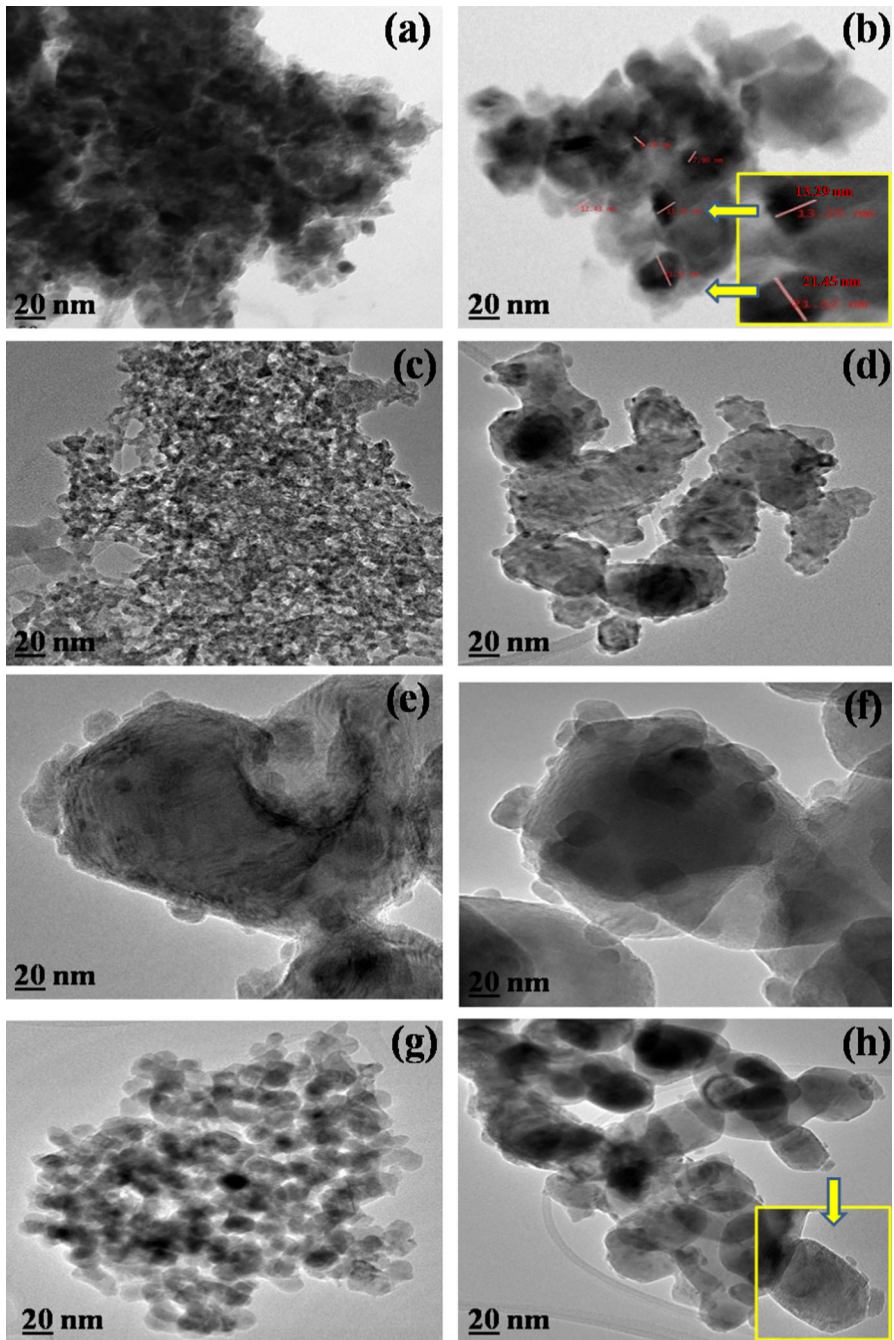


Fig. 7 TEM images of **a–b** AP-CuAl₂O₄, **c–d** APS-CuAl₂O₄, **e–f** MW-CuAl₂O₄, and **g–h** MWS-CuAl₂O₄

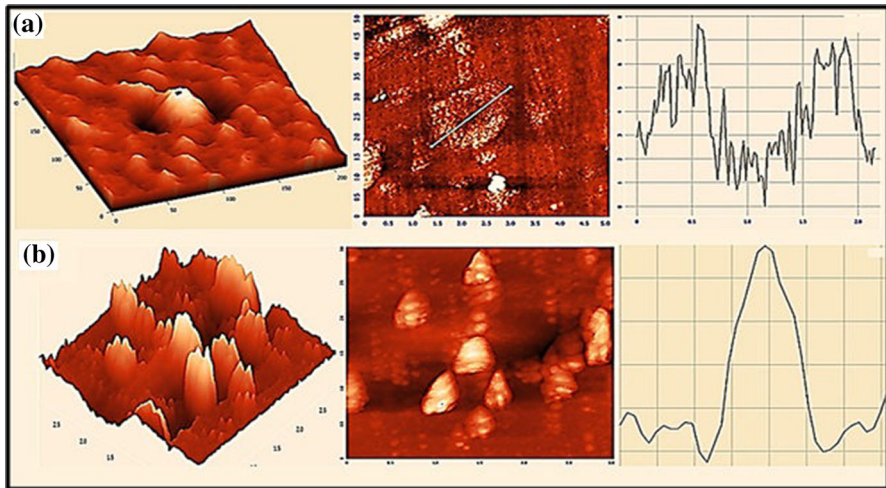


Fig. 8 AFM images of **a** APS-CuAl₂O₄ and **b** MWS-CuAl₂O₄

than their counterpart APS-CuAl₂O₄ NCs. The surface roughness of the APS-CuAl₂O₄ NCs and MWS-CuAl₂O₄ NCs was around 1.36 and 2.85 nm, respectively.

Electrochemical performance

As-synthesized CuAl₂O₄ NCs were tested for their electrochemical performance by CV in 1 M Na₂SO₄ aqueous solution in a three-electrode system. Their CV profiles are presented in Fig. 9. The CV profile of the AP-CuAl₂O₄ NCs was recorded (Fig. 9a) in the scan range of 0–0.9 V with respect to platinum as reference electrode at 10 mV s⁻¹. Redox peaks were not observed in the CV profiles for the AP-CuAl₂O₄ NC electrode, indicating that the specific capacitance of an electrode arose due to an electrical double-layer capacitance. However, the CV curves for the APS-CuAl₂O₄ NCs (Fig. 9b) were recorded in the potential window from – 0.6 to + 1 V, showing nearly rectangular shape, indicating reversible electrochemical reactions and implying electrochemical capacitor behavior. Meanwhile, the CV curves (Fig. 9c & d) for the MW-assisted (MW-CuAl₂O₄ and MWS-CuAl₂O₄) NCs were recorded in the potential window from – 1 to + 1 V, showing two quasireversible electron transfer processes, indicating pseudo-capacitive nature. The specific capacitance of the samples was calculated using the following formula [40]:

$$C = \frac{\int I(V)dV}{(2m\Delta V(V_2 - V_1))},$$

where C is the specific capacitance in F g⁻¹, $I(V)$ is the instantaneous current in A, $\int I(V)dV$ is the total voltammetric charge in C, ΔV is the scan rate in V s⁻¹, and $(V_2 - V_1)$ is the potential window range in V. The highest specific capacitance of 119 F g⁻¹ was observed for the MWS-CuAl₂O₄ NC electrode compared with the other electrodes.

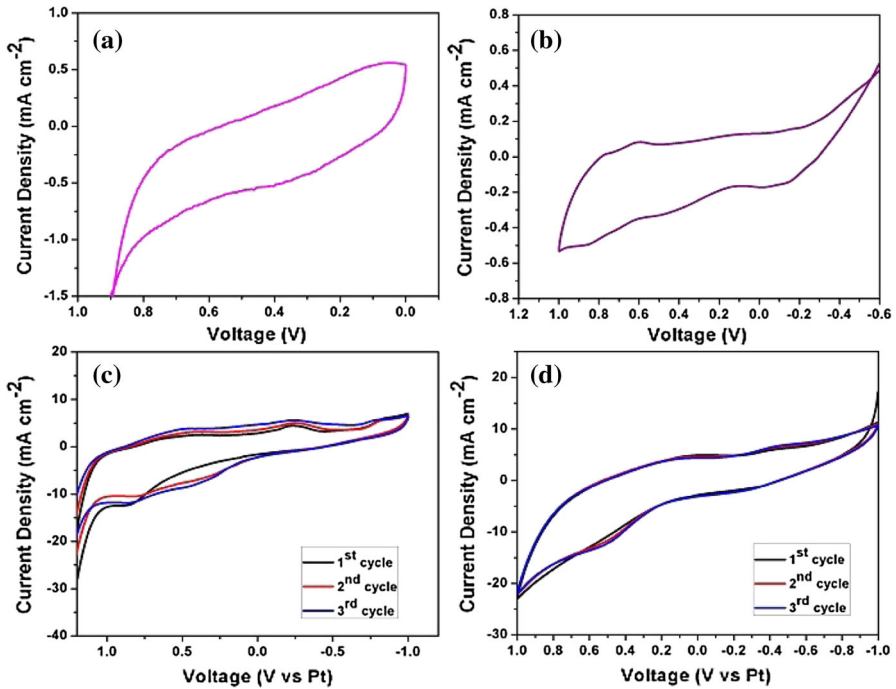


Fig. 9 CV curves of **a** AP-CuAl₂O₄, **b** APS-CuAl₂O₄, **c** MW-CuAl₂O₄, and **d** MWS-CuAl₂O₄ NCs

Supercapacitive properties

Galvanostatic charge/discharge (CP) study of various CuAl₂O₄ NCs was carried out to investigate their supercapacitive behavior. Figure 10a shows the resulting profiles for AP-CuAl₂O₄ NCs at current density of 0.5 mA cm⁻², showing a sudden drop of large potential at the start of the discharge cycle. This occurs because of an internal resistance; the linear variation of potential with time indicates double-layer capacitive behavior, which is caused by charge separation at the electrode–electrolyte interface [41]. Meanwhile, the charge/discharge cycle for the APS-CuAl₂O₄ NCs (Fig. 10b) at the same current density revealed low internal resistance compared with the AP-CuAl₂O₄ NCs. The galvanostatic charge/discharge curves of the MW-assisted (MW-CuAl₂O₄ and MWS-CuAl₂O₄) NCs are depicted in Fig. 10(c & d). The charge/discharge curves are symmetric, further supporting the suggestion that the electrode exhibited electrochemical reversibility and capacitive behavior [42]. Better charge/discharge performance was observed for the MW-assisted (MW-CuAl₂O₄ and MWS-CuAl₂O₄) NCs compared with an AP-assisted NCs, owing to high electrode surface roughness, which enhances the effective utilization area of the electrode. This is in accordance with the AFM results. The specific capacitance of the NCs was calculated using the formula [43]

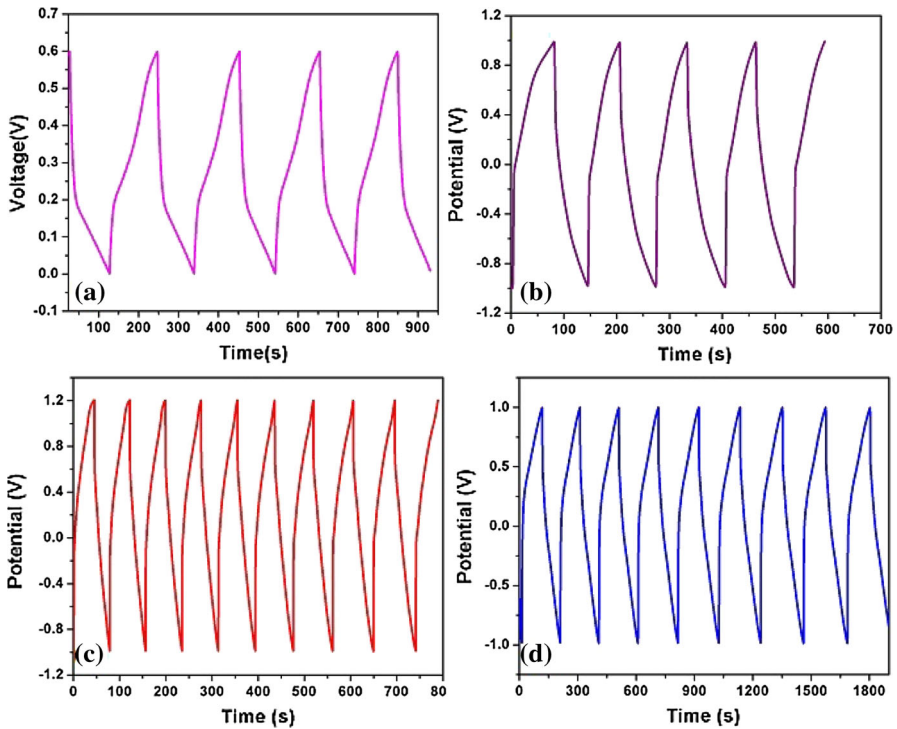


Fig. 10 Charge/discharge performance of **a** AP-CuAl₂O₄, **b** APS-CuAl₂O₄, **c** MW-CuAl₂O₄, and **d** MWS-CuAl₂O₄ NCs

$$C = \frac{I\Delta t}{\Delta Vm},$$

where C is the specific capacitance in F g^{-1} , I is the galvanostatic discharge current in A, Δt is the discharge time in s, ΔV is the voltage range in V, and m is the weight of active material in the electrode in g. The specific capacitance values for the AP-CuAl₂O₄, APS-CuAl₂O₄, MW-CuAl₂O₄, and MWS-CuAl₂O₄ NCs measured at current density of 0.5 mA cm^{-2} were 78, 96, 104, and 125 F g^{-1} , respectively. The poor charge/discharge performance of the electrodes obtained by an AP-assisted method (AP-CuAl₂O₄ and APS-CuAl₂O₄ NCs) compared with the MW-assisted NCs, may be due to their larger crystallite size and lower electrode surface roughness, which would decrease the effective utilization area of the electrode. The MW-assisted (MW-CuAl₂O₄ and MWS-CuAl₂O₄) NCs exhibited longer charge/discharge duration compared with an AP-assisted (AP-CuAl₂O₄ and APS-CuAl₂O₄) NCs, as these electrodes possessed smaller particle size and high surface area and crystallinity with high surface roughness of NCs.

MWS-CuAl₂O₄-catalyzed solvent-free synthesis of xanthenediones

Solvent-free organic transformation reactions have gained noteworthy importance due to their advantages such as eco-friendliness, low cost, facile method, rapid chemical reaction rate, and excellent yield. Therefore, aimed to develop MWS-CuAl₂O₄-catalyzed solvent-free synthesis of xanthenediones. In the present work, solvent-free condensation was investigated based on reaction of aromatic aldehydes with dimedone using MWS-CuAl₂O₄ NCs as nanocatalyst. Next, to optimize the synthesis condition for the MWS-CuAl₂O₄ NCs, xanthenedione derivatives were synthesized with and without (solvent-free) use of solvents using the model reaction under reflux condition. Different solvents such as water, ethanol, ethyl acetate, chloroform, and dichloroethane were chosen for the optimization. The results are presented in terms of reaction time and percent yield in Table 2, revealing that the reaction proceeded satisfactorily with higher yield (87%) and shorter time (2 h), when carried out in solvent-free, green condition compared with the solvent-mediated reaction.

Moreover, the temperature was optimized for the solvent-free, green synthesis of xanthenedione derivatives by varying the reaction temperature to 60, 70, 80, 90, 100, 110, and 120 °C. Figure 11(a) shows the influence of the temperature on the percent synthesis yield. With increasing temperature up to 90 °C, the percent yield of the reaction increased rapidly, but decreased gradually thereafter, revealing the best yield at 90 °C compared with other temperatures. The performance of the MWS-CuAl₂O₄ NCs is compared with reported literature in Table 3, revealing an excellent performance for the present model reaction in terms of reaction time, condition, solvent, and yield of finished product. Consequently, as-prepared MWS-CuAl₂O₄ NCs could be employed as an alternative catalyst for solvent-free synthesis of xanthenediones.

The regeneration and reusability of the MWS-CuAl₂O₄ NCs were also investigated (Fig. 11b), being highly preferable characteristics for a proficient greener process. The recovered NCs were used in the model reaction, adopting an experimental procedure similar to that mentioned in “Experimental” section, being applied in subsequent trials without further purification. The recovery process of the

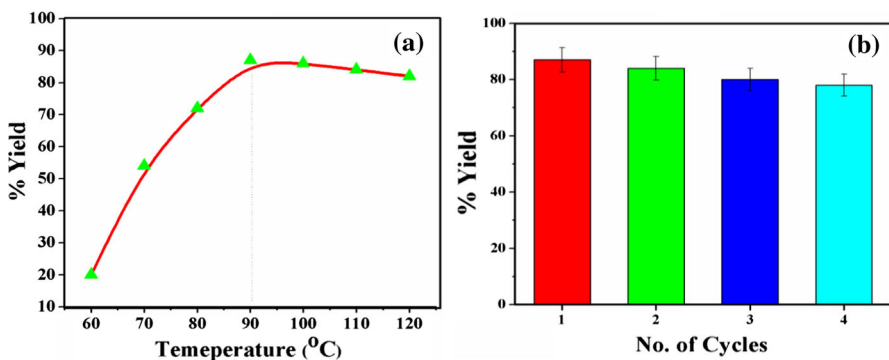


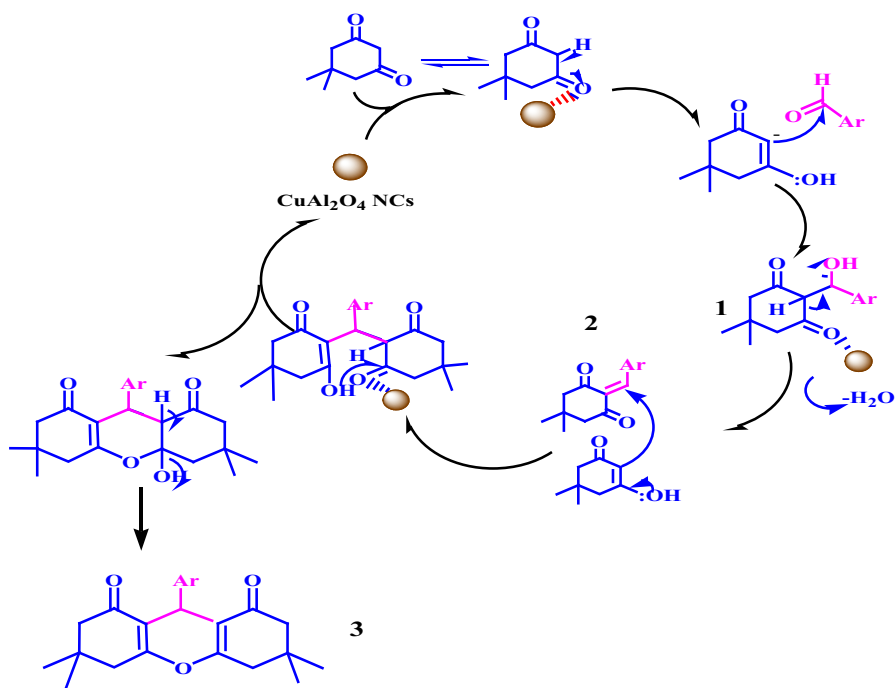
Fig. 11 a Effect of temperature on % yield and b reusability of MWS-CuAl₂O₄ NCs

Table 3 Comparison of different catalysts and conditions with the synthesis presented herein

Entry	Catalyst	Solvent	Condition	Time (min)	Yield (%)	References
1	Fe ³⁺ -montmorillonite	Ethanol	Reflux	360	75	[44]
2	ZrOCl ₂ ·8H ₂ O	Solvent free	Δ, 85 °C	35	96	[45]
3	SiO ₂ -H ₂ SO ₄	H ₂ O	Δ, 65 °C	60	90	[46]
4	Cs _{2.5} H _{0.5} PW ₁₂ O ₄₀	H ₂ O	Δ, 100 °C	30	94	[47]
5	InCl ₃ or P ₂ O ₅	Solvent free	Δ, 100 °C	20	98	[48]
6	Al ₂ O ₃ -OSO ₃ H	Ethanol	Reflux	240	83	[49]
7	SO ₄ ²⁻ /ZrO ₂	Ethanol	Δ, 70 °C	480	90	[50]
8	MWS-CuAl ₂ O ₄	Solvent free	Reflux, 90 °C	120	87	Present work

NCs was facile, efficient, and easy. The recovered NCs exhibited good catalytic activity in up to four cycles of the model reaction. Owing to loss of NCs during the recovery process, a negligible difference was seen in the percent yield of the reaction for constant time period.

A mechanistic rationale for the possible sequence of reactions occurring during formation of products is presented in Scheme 3. Firstly, reactant dimedone was treated with MWS-CuAl₂O₄ NCs to form a dimedone-CuAl₂O₄ complex. This was followed by condensation with one molecule of aromatic aldehyde to form intermediate **1** via aldol condensation. Afterwards, the active methylene group of

**Scheme 3** Mechanism for MWS-CuAl₂O₄-catalyzed synthesis of xanthenedione derivatives

another molecule of dimedone reacted with intermediate **1** through Michael addition to produce intermediate **2**. Intermediate product **2** then underwent intramolecular cyclodehydration to give final product **3**.

Conclusions

Spinel CuAl_2O_4 NCs were synthesized with/without use of sodium dodecyl sulfate by eco-friendly AP and MW-assisted technique and the effects of the synthesis protocol on the structural, morphological, and electrochemical properties were investigated. TEM revealed uniform nanospheres with average particle size of 10 nm for MWS- CuAl_2O_4 NCs, while APS- CuAl_2O_4 NCs were nanograin like with particle size of 17 nm. AFM revealed comparatively higher surface roughness for the MWS- CuAl_2O_4 NCs compared with the APS- CuAl_2O_4 NCs. The synthesis protocols applied had a dominant effect on the physicochemical properties of the spinel CuAl_2O_4 NCs due to their different heating mechanisms. Hence, smaller crystallite and particle sizes, better surface roughness, and high specific capacitance were exhibited by the MWS- CuAl_2O_4 NCs compared with the APS- CuAl_2O_4 NCs. Furthermore, the MWS- CuAl_2O_4 NCs were employed as catalyst for solvent-free, green synthesis of xanthenedione derivatives. The facile experimental protocol, shorter and mild reaction condition, good yield, compatibility with various functional groups, recovery, and reusability of the MWS- CuAl_2O_4 NCs make this approach more environmentally friendly and attractive for synthesis of a variety of these derivatives, thereby contributing to the development of more environmentally benign methods.

Acknowledgements R.G.C. thanks the Science and Engineering Research Board (SERB), India for providing a research grant (no. SB/EMEQ-366/2014) under the scheme “Empowerment and Equity Opportunities for Excellence in Science”.

Compliance with ethical standards

Conflict of interest The authors have no competing financial interests.

Abbreviations

NCs	Nanocomposites
SDS	Sodium dodecyl sulfate
AP	Aqueous precipitation
MW	Microwave
MWS	Microwave-assisted with surfactant (SDS)
APS	Aqueous precipitation with surfactant (SDS)
XRD	X-ray diffraction
FT-IR	Fourier-transform infrared
DRS	Diffuse reflectance spectroscopy
EDS	Energy-dispersive X-ray spectroscopy
XPS	X-ray photoelectron spectroscopy
SEM	Scanning electron microscopy

TEM	Transmission electron microscopy
AFM	Atomic force microscopy
CV	Cyclic voltammetry
RBF	Round-bottomed flask
TLC	Thin-layer chromatography
JCPDS	Joint Committee on Powder Diffraction Standards
SERB	Science and Engineering Research Board

References

1. R. Schlogl, *Angew. Chem. Int. Ed.* **54**, 3465 (2015)
2. M. Climent, A. Corma, S. Iborra, M. Sabater, *ACS Catal.* **4**, 870 (2014)
3. J. Kun-Ming, U. Luesakul, S. Zhao, N. Muangsins, N. Neamati, Y. Jin, J. Lin, *ACS Omega* **2**, 3123 (2017)
4. C. Zou, Z. Zhang, X. Xu, Q. Gong, J. Li, C.D. Wu, *J. Am. Chem. Soc.* **134**, 87 (2012)
5. H. Sun, X. Yang, L. Zhao, T. Xu, J. Lian, *J. Mater. Chem. A* **4**, 9455 (2016)
6. H. Dadhania, D. Raval, A. Dadhania, *Res. Chem. Intermed.* (2017). <https://doi.org/10.1007/s11164-017-3093-2>
7. F. Wang, M. Wei, D. Evans, X. Duan, *J. Mater. Chem. A* **4**, 5773 (2016)
8. S. Kalita, S.J. Saikia, N. Deka, D.C. Deka, H. Mecadon, *Res. Chem. Intermed.* **42**, 6863 (2016)
9. S. Hassanzadeh-Tabrizi, R. Pournajaf, A. Moradi-Faradonbeh, S. Sadeghinejad, *Ceram. Int.* **42**, 14121 (2016)
10. N. Yang, H. Sun, *Coord. Chem. Rev.* **25**, 2354 (2007)
11. A. Wiercinska, *Electrochim. Acta* **55**, 5917 (2010)
12. N. Rajeevan, R. Kumar, D. Shukla, P. Pradyumnan, S. Arora, I. Shvets, *Mater. Sci. Eng. B* **163**, 48 (2009)
13. K.B. Kwak, S.D. Park, S.Y. Yun, J. Yi, *Catal. Commun.* **24**, 90 (2012)
14. J. Yanyan, L. Jinggang, S. Xiaotao, N. Guiling, W. Chengyu, G. Xiumei, *J. Sol Gel Sci. Technol.* **42**, 41 (2007)
15. M. Salavati-Niasari, F. Davar, M. Farhadi, *J. Sol Gel Sci. Technol.* **51**, 48 (2009)
16. W. Lv, L. Zhongkuan, H. Yang, B. Liu, W. Weng, J. Liu, *Ultrason. Sonochem.* **17**, 344 (2010)
17. J. Chandradass, K. Kim, *J. Ceram. Process. Res.* **11**, 96 (2010)
18. C. Ragupathi, J. Vijaya, L. JohnKennedy, M. Bououdina, *Mater. Sci. Semicond. Process.* **24**, 146 (2014)
19. A. Zhihui, L. Zhang, F. Kong, H. Liu, W. Xing, J. Qiu, *Mater. Chem. Phys.* **111**, 162 (2008)
20. E. Nyutu, W. Conner, S. Auerbach, C. Chen, S. Suib, *J. Phys. Chem.* **112**, 1407 (2008)
21. P. Veronesi, C. Leonelli, F. Bondioli, *Powder Technol.* **53**, 42 (2017)
22. S. Menon, K. Choudhari, S. Shivashankar, C. Santhosh, S. Kulkarni, *J. Alloys Compd.* **728**, 1083 (2017)
23. R. Yuvasravana, P. George, N. Devanna, *Mater. Today Proc.* **4**, 10664 (2017)
24. I. Sahu, D. Bisen, R. Sharma, *Res. Chem. Intermed.* **42**, 2791 (2016)
25. M. Shahmirzaee, M. Shafiee Afarani, A. Arabi, A. Nejjad, *Res. Chem. Intermed.* **43**, 321 (2017)
26. A. Pramanik, S. Bhar, *Catal. Commun.* **20**, 17 (2012)
27. W. Lv, B. Liu, Q. Qiu, F. Wang, Z. Luo, P. Zhang, S. Wei, *J. Alloys Compd.* **479**, 480 (2009)
28. J. Tanna, R. Chaudhary, N. Gandhare, A. Rai, S. Yerpude, H. Juneja, *J. Exp. Nanosci.* **11**, 884 (2016)
29. J. Tanna, R. Chaudhary, N. Gandhare, H. Juneja, *Adv. Mater. Lett.* **7**, 933 (2016)
30. D. Ding, M. Long, W. Cai, Y. Wu, D. Wu, *Chem. Commun.* **24**, 3588 (2009)
31. M. Naderi, A. Shamirian, M. Edrisi, *J. Sol Gel Sci. Technol.* **58**, 557 (2011)
32. V. D'Ippolito, B. Giovanni, B. Danilo, P. Lottici, *J. Raman Spectrosc.* **12**, 1255 (2015)
33. F. Ospitali, T. Franca, M. Carla, D. Lonardo, *J. Raman Spectrosc.* **36**, 18 (2005)
34. L. Kock, D. De, D. Waal, *J. Raman Spectrosc.* **38**, 1480 (2007)

35. M. Bouchard, A. Gambardella, J. Raman Spectrosc. **41**, 1477 (2010)
36. G. De Wijs, A. Fang, G. Kresse, Phys. Rev. B **65**, 094305 (2002)
37. G. Moretti, G. Fierro, M. LoJacono, P. Porta, Surf. Interface Anal. **16**, 352 (1990)
38. R. Pan, Y. Wu, Q. Wang, Y. Hong, Chem. Eng. J. **153**, 206 (2009)
39. H. An, H. Yang, Z. Liu, Z. Zhang, LWT Food Sci. Technol. **41**, 1466 (2008)
40. D. Shaikh, P. Rosaiah, O. Hussain, Adv. Sci. Eng. Med. **8**, 140 (2016)
41. D. Dubal, R. Holze, New J. Chem. **37**, 403 (2013)
42. D. Yan, H. Zhang, L. Chen, G. Zhu, Z. Wang, H. Xu, A. Yu, RSC Adv. **4**, 23649 (2014)
43. D. Shaikh, P. Rosaiah, O. Hussain, J. Adv. Chem. **12**, 3919 (2015)
44. A. Romainor, S. Chin, C. Pang, L. Bilung, J. Nanomater. **2014**, 130 (2014)
45. S. Guoyong, B. Wang, H. Luo, L. Yang, Catal. Commun. **8**, 673 (2007)
46. E. Mosaddegh, M. Islami, A. Hassankhani, Arab. J. Chem. **5**, 77 (2012)
47. B. Sadeghi, A. Hassanabadi, E. Taghvatalab, J. Chem. Res. **35**, 707 (2011)
48. A. Thakur, A. Sharma, A. Sharma, Synth. Commun. **46**, 1766 (2016)
49. G. Verma, K. Raghuvanshi, R. Verma, P. Dwivedi, M. Singh, Tetrahedron **67**, 3698 (2011)
50. S. Kahandal, A. Burange, S. Kale, P. Prinsen, R. Luque, R. Jayaram, Catal. Commun. **97**, 138 (2017)